AGU PUBLICATIONS

Geophysical Research Letters

RESEARCH LETTER
10.1002/2014GL060091

Key Points:
- Sea level and earthquake cycle model vertical displacements are compatible
- Thick plates/moderate viscosities reproduce tide gauge rates
- Lateral variations in sea level may be due to fault locking depth changes

Supporting Information:
- Readme
- Text S1
- Table S1
- Figure S1

Correspondence to:
B. R. Smith-Konter and D. T. Sandwell,
brkonter@hawaii.edu;
dsandwell@ucsd.edu

Citation:
Smith-Konter, B. R., G. M. Thornton, and D. T. Sandwell (2014), Vertical crustal displacement due to interseismic deformation along the San Andreas fault: Constraints from tide gauges, *Geophys. Res. Lett.*, *41*, doi:10.1002/2014GL060091.

Received 10 APR 2014
Accepted 12 MAY 2014
Accepted article online 14 MAY 2014

Vertical crustal displacement due to interseismic deformation along the San Andreas fault: Constraints from tide gauges

Bridget R. Smith-Konter[1,2], Garrett M. Thornton[2], and David T. Sandwell[3]

[1]Department of Geology and Geophysics, University of Hawaii at Manoa, Honolulu, Hawaii, USA, [2]Department of Geological Sciences, University of Texas at El Paso, El Paso, Texas, USA, [3]Institute for Geophysics and Planetary Physics, Scripps Institution of Oceanography, La Jolla, California, USA

Abstract Interseismic motion along complex strike-slip fault systems such as the San Andreas Fault System (SAFS) can produce vertical velocities that are ~10 times smaller than horizontal velocities, caused by along-strike variations in fault orientation and locking depth. Tide gauge stations provide a long (50–100 year) recording history of sea level change due to several oceanographic and geologic processes, including vertical earthquake cycle deformation. Here we compare relative sea level displacements with predictions from a 3-D elastic/viscoelastic earthquake cycle model of the SAFS. We find that models with lithospheric structure reflecting a thick elastic plate (>50 km) and moderate viscosities produce vertical motions in surprisingly good agreement with the relative tide gauge uplift rates. These results suggest that sea level variations along the California coastline contain a small but identifiable tectonic signal reflecting the flexure of the elastic plate caused by bending moments applied at the ends of locked faults.

1. Introduction

Vertical crustal deformation that occurs during the earthquake cycle consists of steady interseismic motion punctuated by a step displacement during the earthquake and decaying postseismic deformation [*Burgmann and Thatcher*, 2013]. Vertical tectonic displacements are well documented at subduction zones for several complete earthquake cycles. These signals are up to several meters and are documented in the sea level record as recorded by corals [*Sieh et al.*, 2008]. Transform plate boundaries can also generate vertical deformation, but since most of the fault motion is strike slip, the vertical deformation is generally small (<10 cm) [*Melini et al.*, 2004]. The 1992 Landers and 1999 Hector Mine earthquakes in Southern California produced vertical deformations that were well documented by interferometric synthetic aperture radar (InSAR) and GPS data [i.e., *Massonnet et al.*, 1993; *Fialko et al.*, 2001]. While the largest coseismic and early postseismic signals from these events are largely explained by fault slip in an elastic half-space, the far-field postseismic signals could have resulted from viscoelastic flow in the upper mantle [*Deng et al.*, 1998; *Pollitz et al.*, 2001; *Freed and Burgmann*, 2004].

Earthquake cycle deformation predicted by viscoelastic models is very sensitive to lithosphere rheology (i.e., elastic plate thickness and mantle viscosity) [*Deng et al.*, 1998; *Pollitz et al.*, 2001; *Johnson and Segall*, 2004; *Hetland and Hager*, 2005; *Smith and Sandwell*, 2006]. Along the San Andreas Fault System (SAFS) transform plate boundary, interseismic strain accumulation can cause uplift and subsidence in excess of 3 mm/yr [*Smith and Sandwell*, 2003, 2006]. These vertical deformation patterns exhibit both spatial and temporal variations as a function of lithospheric structure over century-long time scales. GPS and InSAR data, which sample only the past ~30 years of crustal motions and are often contaminated by seasonal and anthropogenic signals [*Wahr et al.*, 2013], thus provide limited constraints.

For the past 50–150 years, sea level change has been semicontinuously recorded by several tide gauge stations along the California coastline adjacent to the SAFS (Figure 1). Tide gauge stations provide a temporal record of sea level change, generally attributed to postglacial rebound, glacial melting, and ocean climate phenomena [e.g., *Douglas*, 1991; *Conrad and Hager*, 1997; *Douglas et al.*, 2001; *Mitrovica et al.*, 2001; *Kuo et al.*, 2004; *Conrad*, 2013]. In this study, we investigate the contribution of vertical tectonic deformation on sea level change recorded over the past 100 years along the California coastline. We compare relative sea level variations and estimates of vertical displacements produced by a 3-D earthquake cycle deformation model that is constrained by geologic slip rates, geodetic velocities, and historical seismic data along the SAFS

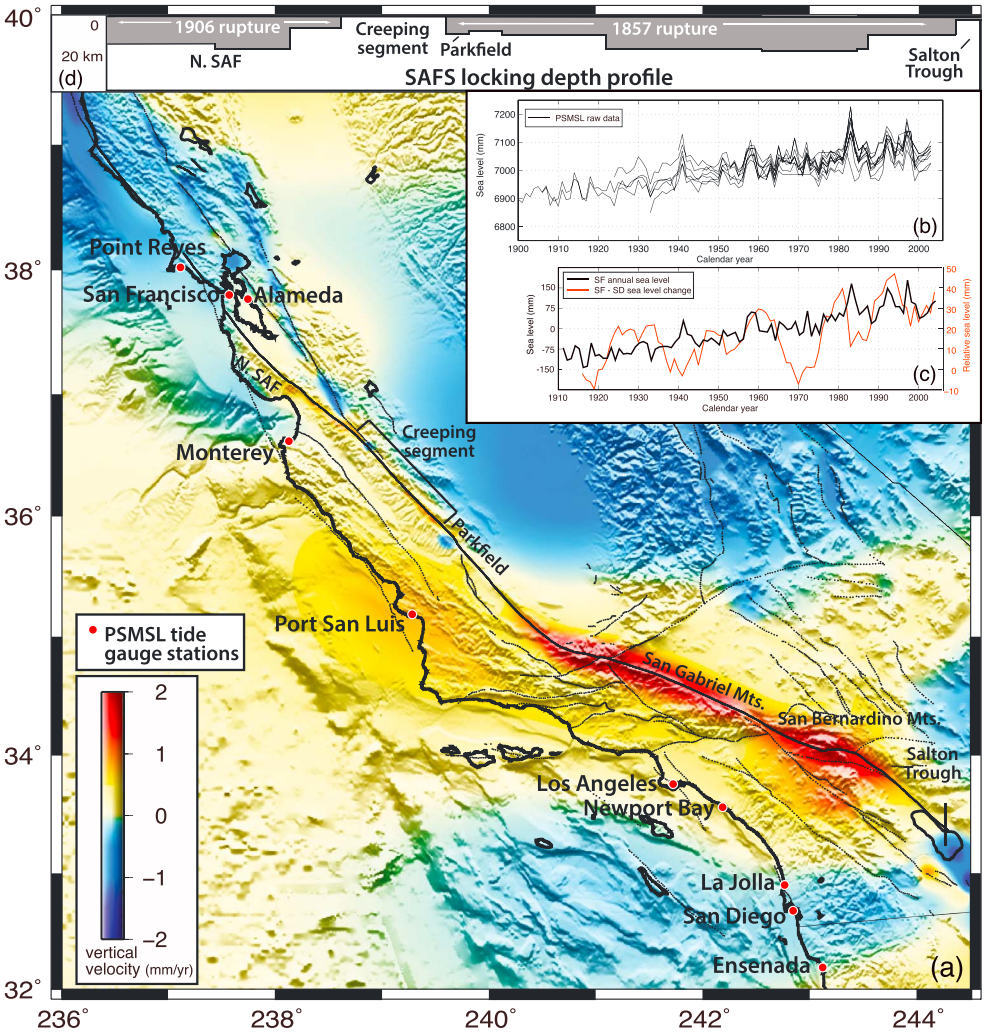

Figure 1. (**a**) Present-day earthquake cycle vertical velocity model of the San Andreas Fault System (see supporting information for model details). Color scale is saturated at ±2 mm/yr. Thick black line represents the primary San Andreas fault; thinner lines represent subsidiary faults. Red circles represent PSMSL tide gauge station locations. (b) Stacked RLR annual time series as obtained from the PSMSL. (c) Example of low-pass filtered (with mean removed) sea level data from the San Francisco station (SF, black, left axis) and relative sea level (RSL) change plotted with respect to San Diego station (SD, red, right axis). (d) Vertical cross section of locking depth variations along the primary San Andreas fault plotted with respect to longitudinal position. Gray zones indicate vertical extent of fault locking.

[*Smith and Sandwell*, 2006]. Spatial and temporal behaviors of vertical deformation arising from elastic plate thickness and mantle viscosity variations are investigated. We find that tide gauge data are indeed sensitive to earthquake cycle deformation of the SAFS, consistent with lithospheric structure represented by a thick elastic plate and a moderate range of viscosities. Moreover, these results suggest that sea level variations along the California coastline contain a small but identifiable tectonic signal reflecting (1) near-field vertical deformation (tens of kilometers from the SAFS) produced from bending fault geometry and (2) far-field vertical deformation (~100 km from the SAFS) generated by major locking depth transitions.

2. Relative Sea Level

Tide gauge data, provided by the Permanent Service for Mean Sea Level (PSMSL, http://www.psmsl.org), measure sea level relative to local vertical crustal motions with high accuracy (<1 mm/yr uncertainties). Major contributions to relative sea level include global sea level rise [*Douglas*, 1991, 1997; *Douglas et al.*, 2001],

glacial isostatic rebound [*Mitrovica and Davis*, 1995; *Miller and Douglas*, 2004], mass redistribution of water due to glacial melting [*Conrad and Hager*, 1997; *Mitrovica et al*., 2001], annual/decadal ocean variability in response to meteorological activity [*Miller and Douglas*, 2007], and vertical land movements due to geological processes, such as ground water extraction, surface water storage, river discharge, and earthquakes [*Melini et al*., 2004; *Argus et al*., 2014; *Amos et al*., 2014]. For this study, we use 9 of 14 PSMSL RLR (revised local reference, referring to PSMSL processing for common datum adjustment) station measurements from Point Reyes, CA to Ensenada, Mexico (Figures 1a and 1b). Five tide gauge stations were omitted due to either a short recording time (i.e., 3 years for the San Mateo station), or numerous, significant gaps in annual sea level measurements [*Douglas*, 2007, also personal communication]. Time series having 1 year gaps were augmented with a 2 year running mean. Sea level records were also adjusted for both the average rise in global sea level (~1.8 mm/yr) [*Douglas et al*., 2001] and a small Global Isostatic Adjustment (GIA) rate for each station (−0.01–0.26 mm/yr, [*Peltier*, 2004]).

Various approaches have been proposed to identify and eliminate oceanographic noise while maintaining rapid crustal motions [i.e., *Larsen et al*., 2003, *Melini et al*., 2004]. Here we compute a 5 year running mean for each data point to smooth out yearly disturbances (Figure 1c). Furthermore, we assume that major ocean climate signals, such as the interannual El Niño related signal, are common to all California stations. To eliminate this signal, we subtract the San Diego residual time series from all the other residual time series. The San Diego station was selected as a reference because of its geographic location with respect to the SAFS, long temporal record, and high data quality (B. Douglas, personal communication, 2009). An example is shown in Figure 1c for a processed sea level record at San Francisco relative to San Diego. We interpret this relative sea level (RSL) difference as being mainly due to vertical tectonic motions related to the earthquake cycle.

3. Vertical Earthquake Cycle Kinematics

To investigate long-term deformation arising from earthquake cycle motions of the SAFS plate boundary, we compute vertical displacements using a 3-D viscoelastic earthquake cycle deformation model [*Smith and Sandwell*, 2004, 2006; *Smith-Konter and Sandwell*, 2009]. This semianalytic model simulates the response of time-dependent dislocations (vertical connected faults) embedded in an elastic plate overlying a viscoelastic half-space, where the restoring force of gravity is also included to accurately model vertical deformation [*Sandwell et al*., 2012]. Interseismic deep slip below locked fault patches generates the first-order orientation and magnitude of the velocity field. Coseismic slip is prescribed along active fault segments at specified epochs. Transient deformation follows each earthquake due to viscoelastic flow in the underlying half-space. The duration of the viscoelastic response, characterized by the Maxwell time, depends primarily on the viscosity of the underlying half-space and the elastic plate thickness. The wavelength of vertical deformation is related to the flexural wavelength (e.g., 440 km wavelength for a 50 km plate thickness).

We use this model to simulate 3-D deformation along the entire the North American-Pacific Plate boundary, spanning roughly a 1000×2000 km region at a 1 km spatial resolution, incorporating 1000 years of earthquake history and applying paleoseismic [e.g., *Grant and Lettis*, 2002], geologic [e.g., *Working Group on California Earthquake Probabilities*, *WGCEP*, 2007], and geodetic constraints [*Smith-Konter et al*., 2011] (see supporting information for parameters and additional model details). The model is purely kinematic in that earthquake cycle slip on 47 fault segments is fully prescribed based on geologic and geodetic data and coseismic slip history spanning the past 1000 years. Apparent locking depths (Figure 1d) were adjusted to match present-day GPS horizontal velocity measurements to an uncertainty of less than 2 mm/yr [*Smith-Konter et al*., 2011]. For the purpose of this study, elastic plate thickness (H) and half-space viscosity (η) are treated as free parameters.

Figure 1 illustrates the present-day (2014) vertical velocity field of the SAFS (assuming $H = 50$ km and $\eta = 1 \times 10^{19}$ Pa s). The present-day vertical velocity field is primarily dominated by interseismic loading (~±3.5 mm/yr), with some time-dependent second-order contributions of postseismic relaxation from recent past earthquakes (on average, $<$ ~0.3 mm/yr). Vertical interseismic deformation results from two processes: (1) misalignment of the fault with respect to the relative plate motion vector and (2) changes in locking depth among the major fault segments (Figure 2) [*Smith and Sandwell*, 2006]. Misalignment, or

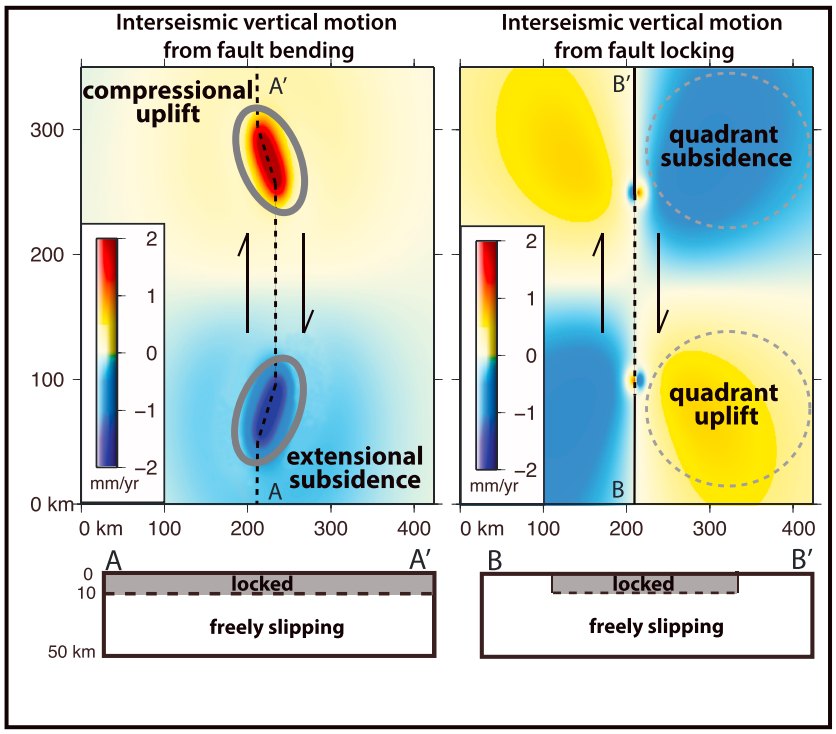

Figure 2. Simple 3-D model (map view) illustrating interseismic vertical motions arising from (left) bending fault geometry and (right) depth transitions from a creeping (freely slipping) fault to a locked fault. In both cases, a locked fault (dashed line, also depicted in vertical cross-sections A-A′ and B-B′) extends from the surface to 10 km depth, embedded within an elastic plate ($H = 50$ km) overlying a viscoelastic half-space ($\eta = 1 \times 10^{19}$ Pa s). A deep slip rate of 40 mm/yr is applied at the base of the locked sections.

bending, of fault geometry generates uplift in compressive regions and subsidence in extensional regions. For example, uplift (~2 mm/yr) in regions of the San Bernardino Mountains and San Gabriel Mountains (~3000 m above sea level) is due to well-defined restraining bends, while subsidence (~ −2 mm/yr) in the Salton Trough (−12 m below sea level) is due to several small releasing bends [i.e., *Williams and Richardson*, 1991; *Smith and Sandwell*, 2003]. In addition, long-wavelength, low-magnitude quadrant lobate patterns of deformation arise from a rapid transition from a creeping (or shallowly locked) fault to a locked fault throughout the earthquake cycle [i.e., *Pollitz et al.*, 2001; *Smith and Sandwell*, 2004]. Along the SAFS, these features result from cyclical locking (Figure 1d) from the Salton Trough to Parkfield and from the North San Andreas/Hayward branches to the Mendicino Triple Junction. South of Parkfield, the upper ~10–15 km of the fault has remained locked since at least the 1857 *M*7.9 Fort Tejon rupture, while the lower part is sliding. A similar effect results from resumed fault locking following the 1906 *M*7.8 San Francisco rupture. This introduces a vertical bending moment at the ends of the locked section that flexes the lithosphere and creates the lobate structure. If another significant event like the 1857 or 1906 ruptures occurs, the moment will be removed and the vertical lobate pattern will relax over the Maxwell time scale [c.f. *Smith and Sandwell*, 2004]. These types of vertical deformations will occur whenever there is a transition in locking depth that occurs over a distance shorter than a ~1/4 flexural wavelength, or ~80 km in this model. Moreover, vertical deformation at distances on the order of 100 km will be most sensitive to SAFS locking depth transitions, while deformation near the fault (approximately tens of kilometers) will be most sensitive to fault bending geometry.

Comparison of these present-day earthquake cycle loading rates with rates of sea level rise observed by tide gauges should ideally yield relative sea level rise consistent with the global average, ~1.8 mm/yr. For example, the San Diego tide gauge observes 2.04 mm/yr of sea level rise [*National Research Council*, 2012], while earthquake cycle loading may contribute 0.2 mm/yr of subsidence at present day, yielding a net rate of sea level rise of 1.84 mm/yr. Similar rates have been verified for La Jolla (1.88 mm/yr), Los Angeles

(1.44 mm/yr), Port San Luis (1.48 mm/yr), and San Francisco (1.82 mm/yr). While long-term earthquake cycle loading rates (discussed next) are a more accurate representation of tectonic contribution to sea level rise, these adjusted sea level rise estimates based on present-day motions provide an important and independent first-order constraint.

4. Results and Discussion

To explore the effects of earthquake cycle deformation on tide gauge measurements, we compare relative vertical displacements derived from sea level measurements to a suite of geodetically constrained displacement models ranging in elastic thickness ($H = 30$, 50, 70 km) and substrate viscosity ($\eta = 8 \times 10^{18}$, 1×10^{19}, 3×10^{19} Pa s). Model time series are constructed by computing annual displacements for the full model grid (reflecting net interseismic, coseismic, and postseismic motions from the entire SAFS) and then extracting vertical displacements at each tide gauge station location. Both model and tide gauge time series are presented relative to San Diego (Figure 3), and model results are plotted with reverse sign, as earthquake cycle induced land movements will inversely affect sea level (i.e., crust moves up, sea level goes down). Note that the San Francisco RSL data appear largely flat over the extent of the 100 year time series; however, these data are plotted with an expanded vertical axis and do vary ~35 mm over the past century; in comparison, the Los Angeles station has a displacement change of over 90 mm over the course of 70 years. It is also worth noting the significant slope variation between RSL time series at the Alameda and San Francisco stations, which are located ~20 km from each other. Douglas [2007] also observed this anomaly, pointing out a 1.1 mm/yr rate change between the two stations, implying greater uplift at Alameda. The Alameda station, which is located ~10 km west of Hayward fault, has the highest relative uplift rate of all the California stations; the source of this behavior is not well understood but may be influenced by other factors beyond earthquake cycle deformation, like bay effects or anthropogenic sources [*Douglas*, 2007, also personal communication].

The slopes of modeled relative vertical displacements are largely controlled by interseismic earthquake cycle motions, following trends similar to those represented by the present-day vertical velocity field (Figure 1), with some small time-dependent variations due to postseismic relaxation. Because San Diego is subsiding at a rate of ~ 0.2 mm/yr on average and remaining locations are subsiding at lesser rates or experiencing uplift, net relative displacements over time are positive, expressed as uplift rates. Displacements from major earthquakes are also evident in the model time series and may be required to explain some of the signatures in the sea level data. For example, some small earthquake displacements can be seen in both models and data (i.e., subtle offsets due to the 1979 Imperial, 1987 Superstition Hills, 1992 Landers, 1999 Hector Mine, and 2004 Parkfield earthquakes). It is important to note that these offsets are presented with respect to deformation observed/modeled at San Diego, so regional events in Southern California will also appear as relative displacements for more northerly located stations.

Models having elastic plate thicknesses >50 km and viscosities spanning 8×10^{18} to 3×10^{19} Pa s produce vertical displacements that explain the sloping trends in the RSL record to a high degree of accuracy at nearly all stations. Visual inspection of model time series reveals a surprisingly significant effect of a thick versus thin elastic plate on long-term uplift rates; small changes in uplift rates can also be expected from viscosity variations; however, the model is not as sensitive to this parameter given the absence of recent major earthquakes. We performed a linear regression analysis to estimate multidecadal uplift rates for each RSL and model time series. RSL-derived rates were also verified by independent estimates provided in a recent National Research Council report on sea level rise [*National Research Council*, 2012]. Assuming a nominal viscosity of 1×10^{19} Pa s (Figure 4a), our results suggest that a thin elastic plate (30 km) primarily yields uplift rates that are considerably larger (mean residual of −1.4 mm/yr) relative to the RSL-derived rates. A 50 km elastic thickness also overpredicts RSL uplift rates, but much less significantly (mean residual of −0.37 mm/yr). A thick (70 km) elastic plate fits RSL uplift rates best for six of the nine stations, with a mean residual of 0.08 mm/yr. Moreover, a thicker plate provides an improved fit to the tide gauge data, with a remarkably good match to the La Jolla, San Francisco, Newport Beach, Monterey, and Port San Luis stations. Furthermore, of the three models presented here, the model representing a thin plate is also the least preferred by previous GPS/geologic data analyses [*Smith and Sandwell*, 2006; *Tong et al.*, 2014]. This model poorly predicts the RSL trends, with the exception of the Alameda station, where it appears to fit quite well; as noted above, however, the Alameda

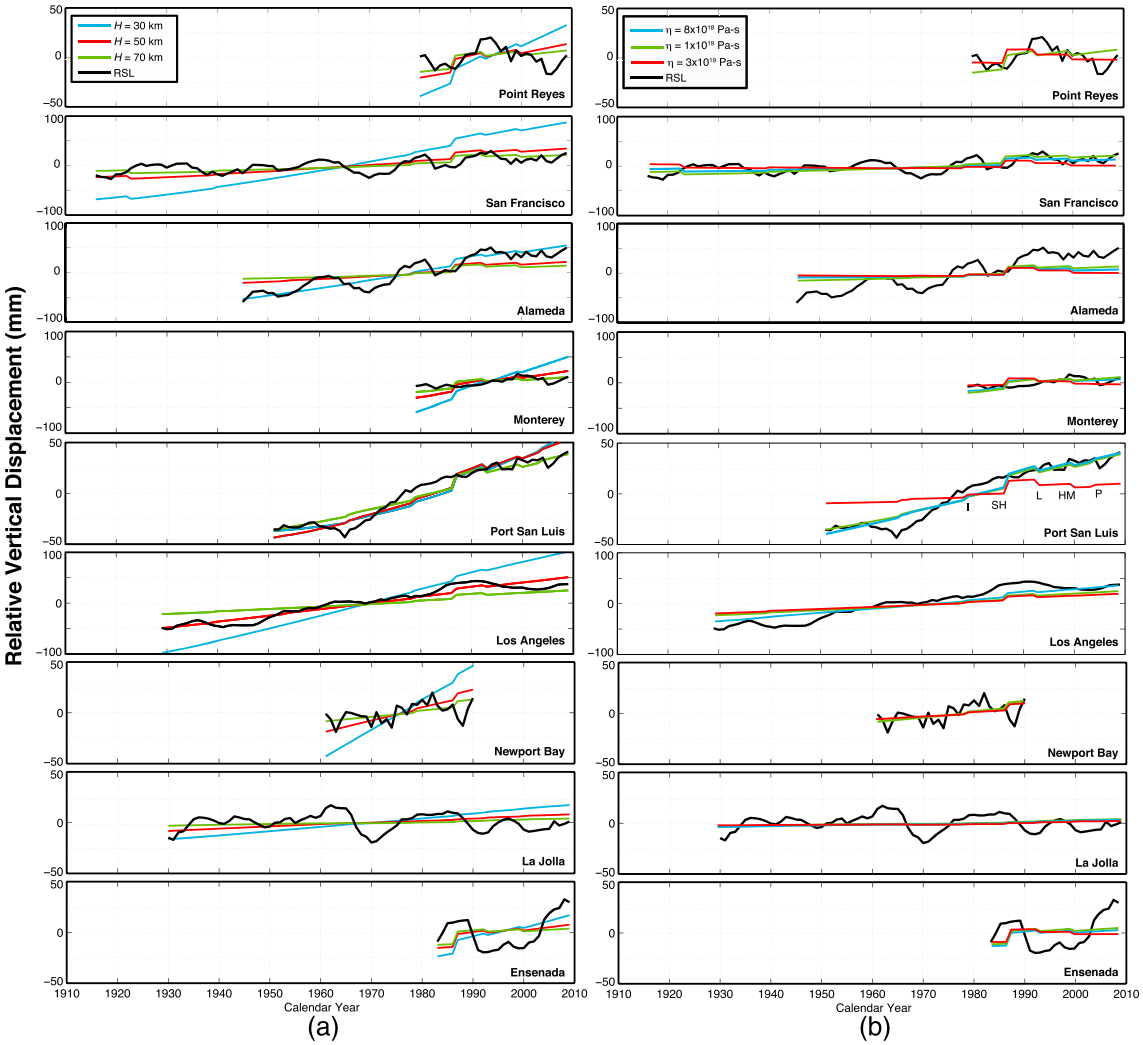

Figure 3. Relative tide gauge and vertical model displacement time series. Tide gauge relative sea level (RSL, black line) data and models are plotted with respect to the San Diego station motions, with the mean removed. (a) Model results (assuming a constant viscosity of $\eta = 1 \times 10^{19}$ Pa s) demonstrating the behavior of three different elastic plate thicknesses: 30 km (blue), 50 km (red), and 70 km (green). (b) Model results (assuming a constant elastic plate thickness of $H = 70$ km) demonstrating the behavior of three different viscosities: 8×10^{18} Pa s (blue), 1×10^{19} Pa s (green), and 3×10^{19} Pa s (red). Note that green lines for both sets of plots represent the same nominal model ($\eta = 1 \times 10^{19}$ Pa s and $H = 70$ km). Coseismic vertical offsets with respect to San Diego are labeled in the Port San Luis panel (I = 1979 Imperial earthquake, SH = 1987 Superstition Hills earthquake, L = 1992 Landers earthquake, HM = 1999 Hector Mine earthquake, and P = 2004 Parkfield earthquake).

station uplift rate is unusually large and may be an artifact of unmodeled phenomena. Geologic uplift rates (~0.6 mm/yr) [*Lienkaemper and Borchardt*, 1996] along the nearby Hayward fault cannot completely account for this large rate of uplift.

We also evaluated the effect of mantle viscosity on long-term uplift rates, assuming a nominal thick elastic plate (70 km) (Figure 4b). Uplift rates resulting from these models indicate that viscosities of 8×10^{18}–1×10^{19} Pa s fit nearly the entire data set (six of nine stations); however a larger viscosity (3×10^{19} Pa s) provides an optimal fit to tide gauge data recorded at Point Reyes and Newport Beach. We note that the variance in uplift rates at the La Jolla station is nearly indistinguishable for any of the parameter combinations due to the proximity of this station to San Diego. Mean residual uplift rates for the three viscosity models are 0.13 mm/yr ($\eta = 8 \times 10^{18}$ Pa s), 0.08 mm/yr ($\eta = 1 \times 10^{19}$ Pa s), and 0.53 mm/yr ($\eta = 3 \times 10^{19}$ Pa s).

These results illustrate how the wavelength and time scale of vertical deformation are largely dependent upon the elastic plate thickness and modestly dependent on half-space viscosity in the absence of major recent earthquakes [*Pollitz et al.*, 2001; *Johnson and Segall*, 2004; *Hetland and Hager*, 2005]. Increasing the

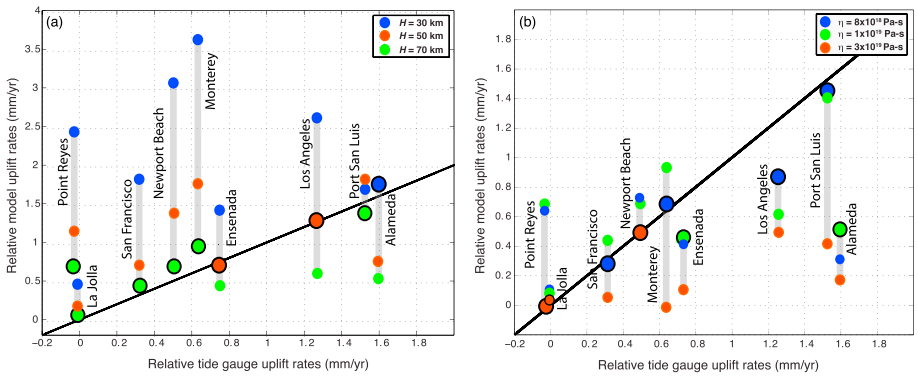

Figure 4. Comparison of tide gauge and model-determined multidecadal relative uplift rates for each station. (a) Model results (viscosity of $\eta = 1 \times 10^{19}$ Pa s) as a function of elastic plate thickness. (b) Model results (elastic plate thickness of $H = 70$ km) as a function of viscosity. Note that plots have different vertical axes and that green circles represent the same nominal model ($\eta = 1 \times 10^{19}$ Pa s and $H = 70$ km). Vertical grey bars serve as visual markers that group model results from each tide gauge location. The solid black lines represent the ideal 1:1 ratio between model and data. Larger circles with a black outline represent the best fitting model for each trial shown.

plate thickness from 30 km to 70 km, for example, has two effects. First, the wavelength of the deformation pattern increases. Second, the amplitude increases because in all the models the locking depths remain constant; thus, the increasing plate thickness increases the length of the moment arm applied at the transition in the locking depth. Furthermore, relaxation time scales of crustal loading play an important role in viscoelastic models. For example, previous work using an epoch-year GPS velocity model reflecting tectonic loading due to postseismic recovery limited to the past ~20 years suggested a preference for models derived from a thick elastic plate (>60 km) [*Smith and Sandwell*, 2006; *Tong et al*., 2014]. Alternatively, other studies report estimates of elastic thickness of 23–46 km based on isostatic rebound from the draining of pluvial lakes and 30 years of leveling data of the Basin and Range [*Iwasaki and Matsu'ura*, 1982; *Nishimura and Thatcher*, 2003]. Thus, a thick ~60 km elastic plate result may be an artifact of the relatively short observation period, combined with a modest contribution of viscoelastic relaxation spanning this period. This value is in agreement with the 40–100 km estimate of *Johnson and Segall* [2004] but is at the high end of elastic thicknesses inferred from postseismic deformation [e.g., *Thatcher and Pollitz*, 2008; *Wright et al*., 2013]. The variability of these collective results highlights the need for additional vertical observations of crustal motion, including those of sea level changes, developed over even longer time spans (>20 years).

Direct comparison of vertical geologic, geodetic, and sea level rates at several sites yield agreement in terms of the sense of vertical motion (relative uplift with respect to San Diego); however, large magnitude variations exist. For example, in Los Angeles (0.6–1.3 mm/yr predicted by our preferred models), the relative uplift rate is 1.3 mm/yr (RSL), 0.1 mm/yr (geodetic, EarthScope PBO station PVRS), and 0.7 mm/yr (geologic, *Niemi et al*. [2008]). In Northern California along the San Francisco peninsula (0.1–0.7 mm/yr model rates), the relative uplift rate is 0.3 mm/yr (RSL), 0.7 mm/yr (geodetic, EarthScope PBO station P177), and 0.2–0.4 mm/yr (geologic, *Grove et al*. [2010]). Near Monterey (0.6–1.7 mm/yr model rates), the relative uplift rate is 0.65 mm/yr (RSL), 1.0 mm/yr (geodetic, EarthScope PBO station P210), and ~1 mm/yr (geologic, *Burgmann et al*. [1994]). At Port San Luis (0.4–1.8 mm/yr model rates), the relative uplift rate is 1.5 mm/yr (RSL), 1.6 mm/yr (geodetic, EarthScope PBO station P523), and 0.3 mm/yr (geologic, *Niemi et al*. [2008]).

While these results suggest that RSL data contain a tectonic signal relating to the earthquake cycle, unmodeled phenomena, also present in the data, require further inspection. Anomalous trends could result from unexplained instrumental datum shifts [*Larsen et al*., 2003]. Short-wavelength effects of bay geometry, ground water depletion, and surface water storage [*Amos et al*., 2014; *Argus et al*., 2014] are not included in our analysis. Furthermore, we do not account for deformation due to small earthquakes (<*M*6) or dipping fault geometry [*Fuis et al*., 2012], the latter of which could vary vertical uplift rates along the coastline by as much as ~ 0.5 mm/yr. In this study, we also made several approximations for eliminating signals within the tide gauge data that are considered "nontectonic" (not arising from earthquake cycle deformation). Uncertainty in signals like the GIA due to regional heterogeneous viscosity structure [*James et al*., 2000] could propagate into our analysis.

5. Conclusions

This study investigated the long-term source of tectonic deformation evident in sea level change recorded over the past 100 years along the California coastline. Using coastal tide gauge time series data, we explored the agreement between sea level changes and vertical displacement trends produced by a 3-D earthquake cycle deformation model that is constrained by geologic slip rates, geodetic velocities, and historical seismic data along the San Andreas Fault System. Models with elastic plate thicknesses of $>$50 km and viscosities of 8×10^{18}–3×10^{19} Pa s produce displacements at tide gauge locations that explain the vertical trends in the sea level record to a high degree of accuracy at nearly all stations. The preference for a thick (50+ km) elastic plate resulting from previous studies utilizing the horizontal GPS velocity field along the SAFS further corroborates these results.

There are several important implications of this analysis. First, the flexure of the elastic plate caused by bending moments applied at the ends of locked faults is evident in tide gauge observations. Such lateral variations in sea level generated by the earthquake cycle process may have significant bearing on studies of past oceanographic behavior and glacial melting. Second, when the next major SAFS earthquake occurs, the current GPS array will be ideal for mapping the lobate deformation pattern both spatially and temporally. Furthermore, the large-scale present-day lobate pattern should also be evident in the GPS data today [*Shen et al*., 2011; *Thornton and Smith-Konter*, 2011], although the vertical rate is small. Earthquake cycle contributions of vertical deformation in California should also be considered by future hydrological studies [*Amos et al*., 2014; *Argus et al*., 2014]. Moreover, these results suggest that tide gauge data are sensitive to strike-slip earthquake cycle deformation and can provide reliable vertical crustal velocities to better probe the rheology of the lithosphere and upper mantle.

Acknowledgments
We thank Roland Burgmann and an anonymous reviewer for their comments and suggestions for clarifying this manuscript. We also thank Bruce Douglas for his helpful discussions regarding usage and application of the tide gauge data used in this study. We thank Clint Conrad for an informative internal review of this manuscript. This research was supported by the National Science Foundation (EAR-0838252, EAR-1147427 and EAR-1147435). Tide gauge data were provided by the Permanent Service for Mean Sea Level (http://www.psmsl.org). This research is also based on data provided by the Plate Boundary Observatory operated by UNAVCO for EarthScope (www.earthscope.org) and supported by the National Science Foundation (EAR-0350028 and EAR-0732947).

The Editor thanks Roland Burgmann and an anonymous reviewer for their assistance in evaluating this paper.

References

Amos, C. B., P. Audet, W. C. Hammond, R. Burgmann, I. A. Johanson, and G. Blewitt (2014), Uplift and seismicity driven groundwater depletion in central California, *Nature*, doi:10.1038/nature13275.

Argus, D. F., Y. Fu, and F. W. Landerer (2014), Seasonal variation in total water storage in California inferred from GPS observations of vertical land motion, *Geophys. Res. Lett.*, *41*, 1971–1980, doi:10.1002/2014GL059570.

Burgmann, R., and W. Thatcher (2013), Space geodesy: A revolution in crustal deformation measurements of tectonic processes, in *The Web of Geological Advances, Impacts and Interactions: Geol. Soc. Am. Spec. Pap.*, vol. 500, edited by M. E. Bickford, pp. 397–430, doi:10.1130/2013.2500(12).

Burgmann, R., R. Arrowsmith, T. Dumitru, and R. McLaughlin (1994), Rise and fall of the southern Santa Cruz Mountains, California, from fission tracks, geomorphology, and geodesy, *J. Geophys. Res.*, *99*, 20,181–20,202, doi:10.1029/94JB00131.

Conrad, C. (2013), The solid Earth's influence on sea level, *GSA Bull.*, *125*(7/8), doi:10.1130/B30764.1.

Conrad, C., and B. Hager (1997), Spatial variations in the rate of se level rise caused by the present-day melting of glaciers and ice sheets, *Geophys. Res. Lett.*, *24*, 1503–1506, doi:10.1029/97GL01338.

Deng, J., M. Gurnis, H. Kanamori, and E. Hauksson (1998), Viscoelastic flow in the lower crust after the 1992 Landers, California, earthquake, *Science*, *282*, 1689–1692.

Douglas, B. (1991), Global sea level rise, *J. Geophys. Res.*, *96*, 6981–6992, doi:10.1029/91JC00064.

Douglas, B. (1997), Global sea level rise: A redetermination, *Surv. Geophys.*, *18*, 279–292.

Douglas, B. (2007), Remarks on the sea level records of the West Coast of North America. [Available at http://www.psmsl.org/products/commentaries/west_coast_north_america.pdf.]

Douglas, B., M. Kearney, and S. Leatherman (2001), *Sea Level Rise*, 232 pp., Academic Press, San Diego, Calif.

Fialko, Y., M. Simons, and D. Agnew (2001), The complete (3-D) surface displacement field in the epicentral area of the 1999 Mw 7.1 Hector Mine earthquake, California, from space geodetic observations, *Geophys. Res. Lett.*, *28*, 3036–3066.

Freed, A. M., and R. Burgmann (2004), Evidence of power-law flow in the Mojave desert mantle, *Nature*, *430*, 548–551, doi:10.1038/nature02784.

Fuis, G. S., D. S. Scheirer, and V. E. Langenheim (2012), A new perspective on the geometry of the San Andreas fault in Southern California and its relationship to lithospheric structure, *Bull. Seismol. Soc. Amer.*, *102*, 236–251, doi:10.1785/0120110041.

Grant, L. B., and W. R. Lettis (2002), Introduction to the special issue on paleoseismology of the San Andreas Fault System, *Bull. Seismol. Soc. Am.*, *92*, 2552–2554.

Grove, K., L.S. Sklar, A. M. Scherer, G. Lee, and J. Davis (2010), Accelerating and spatially-varying crustal uplift and its geomorphic expression, San Andreas Fault zone north of San Francisco, California, *Tectonophysics*, *495*, 256–268, doi:10.1016/j.tecto.2010.09.034.

Hetland, E. A., and B. H. Hager (2005), Postseismic and interseismic displacements near a strike-slip fault: A 2D theory for general linear viscoelastic rheologies, *J. Geophys. Res.*, *110*, B10401, doi:10.1029/2005JB003689.

Iwasaki, T., and M. Matsu'ura (1982), Quasi-static crustal deformations due to a surface load, *J. Phys. Earth*, *30*, 469–508.

James, T. S., J. J. Clague, K. Wang, and I. Hutchinson (2000), Postglacial rebound at the northern Cascadia subduction zone, *Quat. Sci. Rev.*, *19*, 1527–1541.

Johnson, K. M., and P. Segall (2004), Viscoelastic earthquake cycle models with deep stress-driven creep along the San Andreas Fault System, *J. Geophys. Res.*, *109*, B10403, doi:10.1029/2004JB003096.

Kuo, C. Y., C. K. Shum, A. Braun, and J. X. Mitrovica (2004), Vertical crustal motion determined by satellite altimetry and tide gauge data in Fennoscandia, *Geophys. Res. Lett.*, *31*, L01608, doi:10.1029/2003GL019106.

Larsen, C. F., K. A. Echelmeyer, J. T. Freymueller, and R. J. Motyka (2003), Tide gauge records of uplift along the northern Pacific-North American plate boundary, 1937 to 2001, *J. Geophys. Res.*, *108*(B4), 2216, doi:10.1029/2001JB001685.

Lienkaemper, J. J., and G. Borchardt (1996), Holocene slip rate of the Hayward fault at Union City, California, *J. Geophys. Res.*, *101*, 6099–6108, doi:10.1029/95JB01378.
Massonnet, D., M. Rossi, C. Carmona, F. Adragna, G. Peltzer, K. Feigl, and T. Rabaute (1993), The displacement field of the Landers earthquake mapped by radar interferometry, *Nature*, *364*, 138–142.
Melini, D., A. Piersanti, G. Spada, G. Soldati, E. Casarotti, and E. Boschi (2004), Earthquakes and relative sea level changes, *Geophys. Res. Lett.*, *31*, L09601, doi:10.1029/2003GL019347.
Miller, L., and B. Douglas (2004), Mass and volume contributions to twentieth-century global sea level rise, *Nature*, *428*, 406–409, doi:10.1038/nature02309.
Miller, L., and B. Douglas (2007), Gyre-scale atmospheric pressure variations and their relation to 19th and 20th century sea level rise, *Geophys. Res. Lett.*, *34*, L16602, doi:10.1029/2007GL030862.
Mitrovica, J. X., and J. L. Davis (1995), Present-day postglacial sea level changes far from the late Pleistocene ice sheets: Implications for recent analyses of tide gauge records, *Geophys. Res. Lett.*, *22*, 2529–2532, doi:10.1029/95GL02240.
Mitrovica, J., M. Tamisiea, J. Davis, and G. Milne (2001), Recent mass balance of polar ice sheets inferred from patterns of global sea-level change, *Nature*, *409*, 1026–1029.
National Research Council (2012), *Sea-Level Rise for the Coasts of California, Oregon, and Washington: Past, Present, and Future*, The National Academies Press, Washington, D. C.
Niemi, D., M. Oskin, and T. Rockwell (2008), Southern California earthquake center geologic vertical motion database, *Geochem. Geophys. Geosyst.*, *9*, Q07010, doi:10.1029/2008GC002017.
Nishimura, T., and W. Thatcher (2003), Rheology of the lithosphere inferred from postseismic uplift following the 1959 Hebgen Lake earthquake, *J. Geophys. Res.*, *108*(B8), 2389, doi:10.1029/2002JB002191.
Peltier, W. R. (2004), Global glacial isostasy and the surface of the ice-age Earth: The ICE-5G(VM2) model and GRACE, *Ann. Rev. Earth. Planet. Sci.*, *32*, 111–149.
Pollitz, F. F., C. Wicks, and W. Thatcher (2001), Mantle flow beneath a continental strike-slip fault: Postseismic deformation after the 1999 Hector Mine earthquake, *Science*, *293*, 1814–1818.
Sandwell, D. T., S. D. Barbot, C. A. Williams, A. Freed, S. Ellis, M. Huang, and B. Smith-Konter (2012), Investigations into effects of different modeling codes and rheology on predicted coseismic and postseismic surface deformation, *2012 SCEC Annual Meeting*, Palm Springs, Calif.
Shen, Z. K., R. W. King, D. C. Agnew, M. Wang, T. A. Herring, D. Dong, and P. Fang (2011), A unified analysis of crustal motion in southern California, 1970–2004: The SCEC crustal motion map, *J. Geophys. Res.*, *116*, B11402, doi:10.1029/2011JB008549.
Sieh, K. D. H., A. J. Natawidjaja, C. Meltzner, H. Shen, K. L. I. Cheng, B. W. Suwargadi, J. Galetzka, B. Philibosian, and R. L. Edwards (2008), Earthquake supercycles inferred from sea-level changes recorded in the corals of West Sumatra, *Science*, *322*, 1674–1678.
Smith, B., and D. T. Sandwell (2003), Coulomb stress accumulation along the San Andreas Fault System, *J. Geophys. Res.*, *108*(B6), 2296, doi:10.1029/2002JB002136.
Smith, B., and D. T. Sandwell (2004), A 3-D semi-analytic viscoelastic model for time-dependent analysis of the earthquake cycle, *J. Geophys. Res.*, *109*, B12401, doi:10.1029/2004JB003185.
Smith, B., and D. T. Sandwell (2006), A model of the earthquake cycle along the San Andreas Fault System for the past 1000 years, *J. Geophys. Res.*, *111*, B01405, doi:10.1029/2005JB003703.
Smith-Konter, B., and D. T. Sandwell (2009), Stress evolution of the San Andreas Fault System: Recurrence interval versus locking depth, *Geophys. Res. Lett.*, *36*, L13304, doi:10.1029/2009GL037235.
Smith-Konter, B., D. T. Sandwell, and P. Shearer (2011), Locking depths estimated from geodesy and seismology along the San Andreas Fault System: Implications for seismic moment release, *J. Geophys. Res.*, *116*, B06401, doi:10.1029/2010JB008117.
Thatcher, W., and F. F. Pollitz (2008), Temporal evolution of continental lithosphere strength in actively deforming regions, *GSA Today*, *18*, 4–11, doi:10.1130/GSAT01804-5a.1.
Thornton, G., and B. Smith-Konter (2011), Modeling vertical deformation along the San Andreas Fault System using geodetic, geologic, groundwater, and tide gauge data, *Abstract G23B-01 presented at the 2011 Fall Meeting*, AGU, 5-9 Dec., San Francisco, Calif.
Tong, X., B. Smith-Konter, and D. T. Sandwell (2014), Is there a discrepancy between geological and geodetic slip rates along the San Andreas Fault System?, *J. Geophys. Res. Solid Earth*, *119*, 2518–2538, doi:10.1002/2013JB010765.
Wahr, J., S. A. Khan, T. van Dam, L. Liu, J. H. van Angelen, M. R. van den Broeke, and C. M. Meertens (2013), The use of GPS horizontals for loading studies, with applications to northern California and southeast Greenland, *J. Geophys. Res. Solid Earth*, *118*, 1795–1806, doi:10.1002/jgrb.50104.
Williams, C. A., and R. M. Richardson (1991), A rheologically layered three-dimensional model of the San Andreas Fault in central and southern California, *J. Geophys. Res.*, *96*, 16,597–16,623, doi:10.1029/91JB01484.
Working Group on California Earthquake Probabilities (WGCEP) (2007), The Uniform California Earthquake Rupture Forecast, Version 2 (UCERF 2), *U.S. Geol. Surv. Open File Rep.*, 2007-1473.
Wright, T. J., J. R. Elliot, H. Wang, and I. Ryder (2013), Earthquake cycle deformation and the Moho: Implications for the rheology of continental lithosphere, *Tectonophysics*, *609*, 504–523, doi:10.1016/j.tecto.2013.07.029.